

Competing orders in Na_xCoO_2 from strong correlations on a two-particle level

Lewin Boehnke and Frank Lechermann

I. Institut für Theoretische Physik, Universität Hamburg, D-20355 Hamburg, Germany

Based on dynamical mean-field theory with a continuous-time quantum Monte-Carlo impurity solver, static as well as dynamic spin and charge susceptibilities for the phase diagram of the sodium cobaltate system Na_xCoO_2 are discussed. The approach includes important vertex contributions to the \mathbf{q} -dependent two-particle response functions by means of a local approximation to the irreducible vertex function in the particle-hole channel. A single-band Hubbard model suffices to reveal several charge- and spin-instability tendencies in accordance with experiment, including the stabilization of an effective kagomé sublattice close to $x=0.67$, without invoking the doping-dependent Na-potential landscape. The in-plane antiferromagnetic-to-ferromagnetic crossover is additionally verified by means of the computed Korringa ratio. Moreover an intricate high-energy mode in the transverse spin susceptibility is revealed, pointing towards a strong energy dependence of the effective intersite exchange.

PACS numbers: 71.27.+a, 71.30.+h, 71.10.Fd, 75.30.Cr

The investigation of finite-temperature phase diagrams of realistic strongly correlated systems is a quite formidable task due to the often tight competition between various low-energy ordering instabilities. In this respect the quasi-twodimensional (2D) sodium cobaltate system Na_xCoO_2 serves as a notably challenging case [1, 2]. Here $x \in [0,1]$ nominally mediates between the $\text{Co}^{4+}(3d^5, S=1/2)$ and $\text{Co}^{3+}(3d^6, S=0)$ low-spin states. Thus the Na ions provide the electron doping for the nearly filled t_{2g} states of the triangular CoO_2 layers up to the band-insulating limit $x=1$. Coulomb correlations with a Hubbard U up to 5 eV for the t_{2g} manifold of bandwidth $W \sim 1.5$ eV [3] are revealed from photoemission [4]. Hence with $U/W \gg 1$ the frustrated metallic system is definitely placed in the strongly correlated regime.

Various different electronic phases and regions for temperature T vs. doping x are displayed in the experimental sodium cobaltate phase diagram (see Fig. 1). For instance a superconducting dome ($T_c \sim 4.5\text{K}$) stabilized by intercalation with water close to $x=0.3$ [5]. Pauli-like magnetic susceptibility is found in the range $x < 0.5$ [1] with evidence for 2D antiferromagnetic (AFM) correlations [2, 6]. For $x > 0.5$ spin fluctuations and increased magnetic response show up for $0.6 < x < 0.67$, including the evolution to Curie-Weiss (CW) behavior [1] for $0.6 < x < 0.75$, and the eventual onset of in-plane ferromagnetic (FM) order. The ordered magnetic structure in the doping range $0.75 < x < 0.9$ with $T_N \sim 19\text{-}27\text{K}$ [7–10] is of A-type AFM for the FM CoO_2 layers. As the local spin-density approximation (LSDA) is not sufficient to account for the AFM-to-FM crossover with x [3], explicit many-body approaches are needed [11–13].

Several theoretical works have dealt with the influence of the sodium arrangements on the electronic properties of Na_xCoO_2 , both from the viewpoint of disordered sodium ions [12] as well as from orderings for certain dopings. [14–16] However, whether such sodium patterns are due to sole (effective) single-particle potentials

or mainly originating from many-body effects within the CoO_2 planes is still a matter of debate [17, 18].

In this letter, we report the fact that a large part of the electronic (spin and charge) phase diagram of sodium cobaltate may be well described within a Hubbard model using realistic dispersions, and without invoking the details of the sodium arrangement. Thereby most of the observed crossovers and instabilities are truly driven by strong correlation effects and cannot be described within weak-coupling scenarios. The theoretical study is elucidating the two-particle correlations in the particle-hole channel computed within dynamical mean-field theory (DMFT) including vertex contributions (for a review see e.g. [19, 20]). So far the latter have been neglected in cobaltate susceptibilities based on LSDA [21, 22] and the fluctuation-exchange approximation [22, 23]. Our dynamical lattice susceptibilities allow to reveal details of the AFM-to-FM crossover with T and of the intriguing charge-ordering tendencies, both in line with recent experimental data [2, 24]. Moreover, insight in the (x, \mathbf{q}) -dependent spin excitations at finite frequency is provided.

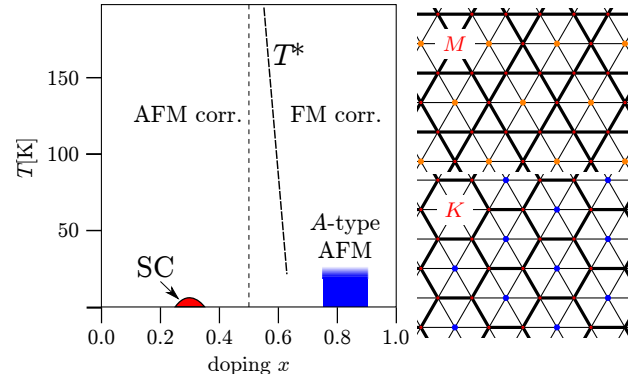


FIG. 1. (color online) Left: Sketched Na_xCoO_2 phase diagram, based on Ref. 2. Right: M - (top) and K - (bottom) point ordering on the triangular lattice.

Since we are mainly interested in the $x > 0.5$ part of the phase diagram, the low-energy band dispersion of sodium cobaltate is described within an a_{1g} -like single-band approach, justified from photoemission [25] and Compton scattering [26] experiments. We primarily focus on the in-plane processes on the effective triangular Co lattice with tight-binding parameters up to 3rd nearest-neighbor (NN) hopping, i.e., $(t, t', t'') = (-202, 35, 29)$ meV [27] for the 2D dispersion. Albeit intersite Coulomb interactions might play a role [13], the canonical modeling was restricted to an on-site Coulomb interaction $U = 5$ eV. Our calculations show that already therefrom substantial nonlocal correlations originate. The resulting Hubbard model on the triangular lattice is solved within DMFT for the local one-particle Green's function $G(\tau_{12}) = -\langle T_\tau c(\tau_1) c^\dagger(\tau_2) \rangle$ with $\tau_{uv} = \tau_u - \tau_v$ and T_τ being the time-ordering operator. The DMFT problem is approached with the continuous-time quantum Monte Carlo methodology [28, 29] in its hybridization-expansion flavor [29] as implemented in the TRIQS package. [30] Additionally we implemented the computation of the impurity two-particle Green's function [31] $G^{(2)}(\tau_{12}, \tau_{34}, \tau_{14}) = -\langle T_\tau c^\dagger(\tau_1) c(\tau_2) c^\dagger(\tau_3) c(\tau_4) \rangle$ to address explicit electron-electron correlations. In the approximation of a purely local particle-hole irreducible vertex, $G^{(2)}$ allows to determine also lattice susceptibilities. [19, 20, 31, 32] These susceptibilities, e.g. for spin (s) and charge (c), written as

$$\chi_{s/c}(i\omega, \mathbf{q}, T) = T^2 \sum_{\nu\nu'} \left(\tilde{\chi}_{s/c, \nu\nu'}^{(0)}(i\omega, \mathbf{q}, T) + v_{s/c, \nu\nu'}(i\omega, \mathbf{q}, T) \right), \quad (1)$$

where ω (ν) marks bosonic (fermionic) Matsubara frequencies, consist of two parts. Namely $\tilde{\chi}_{s/c, \nu\nu'}^{(0)}$ denotes the conventional (Lindhard-like) term, build up from the (renormalized) bubble part, which is mainly capable of detecting Fermi-surface driven instabilities close to $T=0$. On the contrary, the second part $v_{s/c, \nu\nu'}$ (the vertex term) includes properly the energy dependence of the response behaviour due to strong local interactions in real space. It proves important for revealing, e.g. magnetic instabilities at finite T due to the resolution of the two-particle correlations governed by an implicit intersite exchange J . Note that all numerics take advantage of the recently introduced Orthogonal Polynomial representation [31] of one- and two-particle Green's functions to provide the needed high accuracy and to eliminate artifacts often stemming from truncating the Fourier-transformed $G^{(2)}$ in Matsubara space.

Within the first Brillouin zone (BZ) of the triangular coordination with lattice constant a the coherent Γ -point instability signals FM order in the case of χ_s and phase separation for χ_c . Additionally important are here the instabilities at the K - and M -point. The associated orderings give rise to distinct sublattice structures

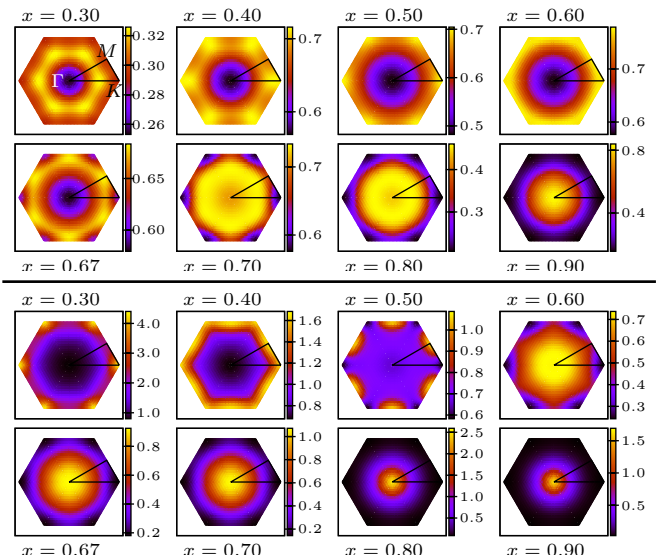


FIG. 2. (color online) Static in-plane charge (top) and spin (bottom) susceptibility $\chi(0, \mathbf{q}, T)$ with doping at $T=386$ K.

in real space (cf. Fig. 1). The M -point ordering leads to a triangular and a kagomé sublattice with lattice constant $a_{\text{eff}} = 2a$, while the K -point ordering establishes a triangular and a honeycomb sublattice with $a_{\text{eff}} = \sqrt{3}a$, respectively.

We will first discuss the static ($\chi_{s/c}(\omega=0, \mathbf{q}, T)$) response (read off from the zeroth bosonic Matsubara frequency), directly reflecting the system's susceptibility to an order of the (\mathbf{q} -resolved) type. The cobaltate intra-layer charge-susceptibility $\chi_c(0, \mathbf{q}, T)$ shows pronounced features in \mathbf{q} space with doping x (see Fig 2). Close to $x=0.3$ our single-band modeling leads to increased intensity inside the BZ, pointing towards longer-range charge-modulation (e.g. 3×3 , etc.) tendencies in real space. That $\text{Na}_{1/3}\text{CoO}_2$ is indeed prone to such 120° -like instabilities has been experimentally suggested by Qian *et al.* [33]. Towards $x=0.5$ the susceptibility for short-range charge modulation grows in χ_c , displaying a diffuse high-intensity distribution at the BZ edge with a maximum at the K -point for $x=0.5$. No detailed conclusive result on the degree and type of charge ordering for the latter composition is known from experiment, however chain-like charge disproportionation that breaks the triangular symmetry is verified [34, 35]. The present single-site approach cannot stabilize such symmetry-breakings, but an pronounced χ_c at the K -point at least inherits some stripe-like separation of the two involved sublattices. Near $x=0.67$, the χ_c maximum has shifted to the M -point, in line with the detection of an effective kagomé lattice from nuclear magnetic resonance (NMR) experiments [24]. For even higher doping, this \mathbf{q} -dependent structuring transmutes into a Γ -point maximum, pointing towards known phase-separating tendencies. [36] Figure 2 also exhibits the x -dependent intra-layer spin sus-

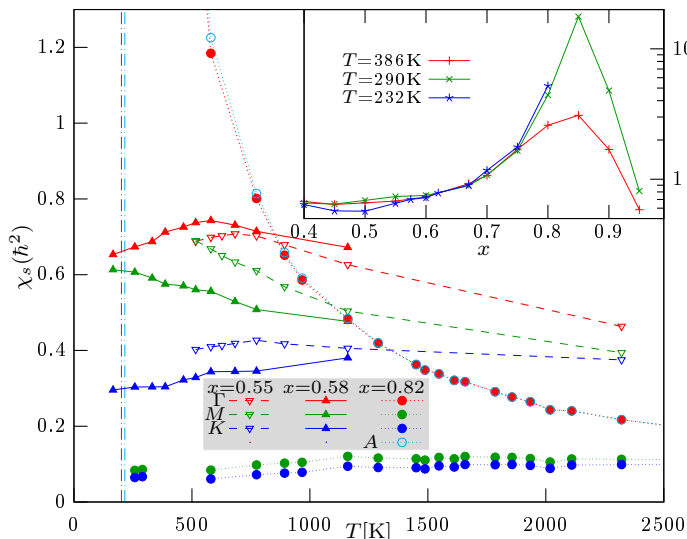


FIG. 3. (color online) Temperature dependence of the spin susceptibility at the Γ , M , and K -point for $x=0.55$, 0.58 , 0.82 . For the latter, values at the A -point are also included. Vertical lines indicate extrapolated transition temperatures for Γ (FM) spin-ordering and A (A-type AFM) spin-ordering respectively for $x=0.82$. The inset shows the doping dependence of the uniform ($\mathbf{q}=\Gamma$) in-plane spin susceptibility χ_s for various T . Note the largely increased magnitude of χ_s for $x \geq 0.75$ in this logscale plot.

ceptibility, starting with strong AFM peaks at $x=0.3$ due to K -point correlations. With reduced intensity these shift to the M -point at $x=0.5$, consistent with different types of spin and charge orderings at this doping level [35]. For $x > 0.5$, $\chi_s(\mathbf{q}, T, 0)$ first develops broad intensity over the full BZ, before forming a pronounced peak at the Γ -point above $x \sim 0.6$. Thus the experimentally observed in-plane AFM-to-FM crossover in the spin response is reproduced.

Lang *et al.* [2] revealed from the Na NMR that this crossover is T -dependent with x , resulting in an energy scale T^* below which AFM correlations are favored (compare Fig. 1). The slope $\partial T^*/\partial x$ turns out negative, in line with the general argument that FM correlations are most often favored at elevated T because of the entropy gain via increased transverse spin fluctuations. In this respect, Fig. 3 shows the (x, T, \mathbf{q}) dependence of the computed χ_s . For $x=0.55$, 0.58 a maximum in the Γ -point susceptibility is revealed, which has been interpreted by Lang *et al.* [2] as the criterion for a change in the correlation characteristics, thereby defining the T^* -line. While the temperature scale exceeds the experimental value in the present mean-field formalism, the qualitatively correct doping behavior of the T^* -line is obtained.

Beyond the experimental findings our calculations allow to further investigate the nature of the magnetic crossover. Fig. 3 reveals that at lower T and x closer to $x=0.5$ the susceptibility at Γ is ousted by the one at

M , while χ_s at K is mostly dispensable. The M susceptibility can be understood due to the proximity of the striped order at $x=0.5$, [1, 17, 37] which is however not realized until much lower temperatures.

The inset of Fig. 3 follows the T -dependent Γ -point susceptibility through a vast doping range. Note the subtle resolution around $x=0.5$ as well as the large exaggeration especially for lower temperatures in the experimentally verified in-plane FM region. The main panel of Fig. 3 additionally shows for $x=0.82$ the spin susceptibility at the A -point (i.e., at $k_z=(0,0,1/2)$ in the BZ), which denotes the A-type AFM order. While Γ and A show CW behavior, the extrapolated transition temperature however is $\sim 7\%$ higher at A than at Γ , verifying the experimental findings of A-type order [7–10]. In the temperature scan we additionally introduced a nearest-layer inter-plane hopping $t_{\perp}=13$ meV [9, 13, 38], however the previous in-plane results are qualitatively not affected by this model extension. Due to known charge disproportionation the inclusion of long-range Coulomb interactions, e.g., via an inter-site V [13, 16], seems reasonable. This was abandoned in the present single-site DMFT approach, resulting generally in reduced charge response. Without V , charge fluctuations are substantially suppressed for large U/W , while the inter-site spin fluctuations are still strong due to superexchange. Aside from the static response, our method allows also access to the dynamic regime. Figure 4 shows the dynamical transverse spin susceptibility for selected x . Note the broad \mathbf{q} -dependence and small excitation energy in the low-doping regime. In contrast, the FM correlations near $x=0.82$ are reflected by strong paramagnon-like gapless excitation at Γ combined with very little weight and rather high excitation energies at AFM wave-vectors. Interestingly, a comparably strong and sharp K -type high-energy excitation (~ 1 eV) for larger x below the onset of in-plane FM order is revealed. Its amplitude is strongest at $x=0.67$ while its energy increases with x and its worthwhile to note that the mode is *neither* visible when ne-

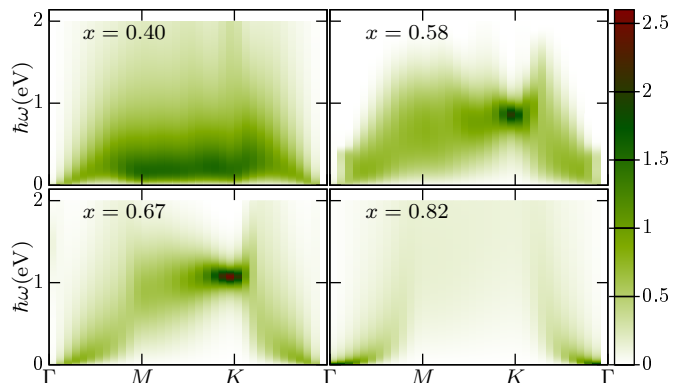


FIG. 4. (color online) Imaginary part of the dynamical spin susceptibility for selected dopings for selected dopings.

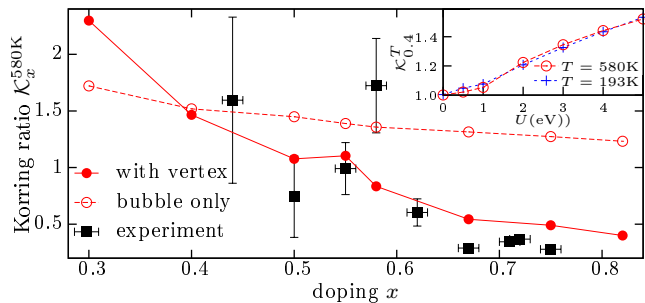


FIG. 5. (color online) Korringa ratio versus doping for $T=580$ K. The experimental data, extracted from Ref. 40 and 2, was obtained for lower temperatures. The inset shows the evolution of the bubble-diagram contribution from the non-interacting ($U=0$) to the fully-interacting ($U=5$ eV) case.

glecting vertex contributions, *nor* in a plain triangular Hubbard model with NN hopping only. Thus it reflects a strong energy dependence of the inter-site exchange coupling $J=J(x, \mathbf{q}, \omega)$, that obviously changes character for $x\sim 0.67$ with \mathbf{q} and ω . The predicted high-energy feature could be probed experimentally and also studied in time-dependent measurements. We propose the use of modern laser-pulse techniques [39] to address this problem.

Experimentally, the evidence for significant $\mathbf{q}\neq 0$ fluctuations is drawn [2, 40] from the Korringa ratio [41–43][44]

$$\begin{aligned} \mathcal{K}_x^T &= \frac{\hbar}{4\pi k_B} \left(\frac{\gamma_e}{\gamma_N} \right)^2 \frac{1}{T_1 T K_S^2} \\ \frac{1}{T_1 T} &= \lim_{\omega \rightarrow 0} \frac{2k_B}{\hbar^2} \sum_{\mathbf{q}} |A(\mathbf{q})|^2 \frac{\Im \chi_s^{-+}(\omega, \mathbf{q}, T)}{\omega} \\ K_S &= \frac{|A(\mathbf{0})| \gamma_e \Re \chi_s^{-+}(0, \mathbf{0}, T)}{\gamma_N \hbar^2} \end{aligned} \quad (2)$$

where $1/T_1$ is the nuclear relaxation rate, K_S the NMR field shift, γ_e (γ_N) the electronic (nuclear) gyromagnetic ratio and $A(\mathbf{q})$ the hyperfine coupling. Roughly speaking, $\mathcal{K}>1$ signals AFM correlations, $\mathcal{K}<1$ points to FM tendencies in χ_s and the term ‘‘Korringa behavior’’ generally denotes the regime $\mathcal{K}(T)\sim 1$. In single-atom unit cells, $A(\mathbf{q})$ becomes \mathbf{q} -independent.

Note that especially $1/T_1$ is numerically expensive, as it requires to calculate χ_s^{-+} on many Matsubara frequencies with subsequent analytical continuation to the real frequency axis for contributions beyond the bubble diagram. Figure 5 finally shows the AFM-to-FM correlation crossover captured by the Korringa-ratio over a wide doping range. The overall agreement with experiment is conclusive. Relevant deviations in the low-doping regime probably originate from the smaller temperatures studied in experiment. The difference at $x=0.58$ might be of the same origin, but since charge ordering occurs for $x>0.5$ which was not included explicitly here, neglecting the \mathbf{q} -dependence of $A(\mathbf{q})$ might be also questionable.[45] One

can see that the bubble-only calculation yields a nearly flat Korringa ratio with doping, thus fails completely in explaining the experimental findings. In particular it does not reflect the strong FM correlations for high doping. This further proves the importance of strong correlations on the two-particle level, asking for substantial vertex contributions. [43] Note that the recently suggested lower-energy effective kagomé model [16] including the affect of charge ordering is not contradicting the present modeling. Since here the effective kagomé lattice naturally shows up and also the key properties of the spin degrees of freedom seem well described on the original triangular lattice.

In summary, the DMFT computation of two-particle observables including vertex contributions based on a realistic single-band Hubbard modeling for Na_xCoO_2 leads to a faithful phase-diagram examination at larger x , including the kagomé-like charge-ordering tendency for $x\sim 0.67$ and the in-plane AFM-to-FM crossover associated with a temperature scale T^* . Thus it appears that many generic cobaltate features are already governed by a canonical correlated model, without invoking the details of the doping-dependent sodium-potential landscape or the inclusion of multi-orbital processes. Of course, future work has to concentrate on quantifying further details of the various competing instabilities (and their mutual couplings) within extended model considerations. Beyond equilibrium physics, we predict a strong energy dependence of the effective inter-site exchange resulting in an K -type high-energy mode around $x=0.67$, which could be probed in experimental studies.

The authors are indebted to O. Parcollet and M. Ferrero for useful discussions on the vertex implementation and calculation. We also like to thank A. Georges, H. Hafermann, A. I. Lichtenstein, O. Peil and C. Piefke for valuable comments. This work was supported by the SPP 1386 and the FOR 1346 of the DFG. Computations were performed at the North-German Supercomputing Alliance (HLRN) and the regional computing center (RRZ) of the University of Hamburg.

-
- [1] M. L. Foo, Y. Wang, S. Watauchi, H. W. Zandbergen, T. He, R. J. Cava, and N. P. Ong, Phys. Rev. Lett. **92**, 247001 (2004)
 - [2] G. Lang, J. Bobroff, H. Alloul, G. Collin, and N. Blanchard, Phys. Rev. B **78**, 155116 (2008)
 - [3] D. Singh, Phys. Rev. B **61**, 13397 (2000)
 - [4] M. Z. Hasan, Y.-D. Chuang, D. Qian, Y. W. Li, Y. Kong, A. Kuprin, A. V. Fedorov, R. Kimmerling, E. Rotenberg, K. Rossnagel, Z. Hussain, H. Koh, N. S. Rogado, M. L. Foo, and R. J. Cava, Phys. Rev. Lett. **92**, 246402 (2004)
 - [5] K. Takada, H. Sakurai, E. Takayama-Muromachi, F. Izumi, R. A. Dilanian, and T. Sasaki, Nature **422**, 53 (2003)
 - [6] T. Fujimoto, G.-Q. Zheng, Y. Kitaoka, R. L. Meng,

- J. Cmaidalka, and C. W. Chu, Phys. Rev. Lett. **92**, 047004 (2004)
- [7] J. Sugiyama, H. Itahara, J. H. Brewer, E. J. Ansaldo, T. Motohashi, M. Karppinen, and H. Yamauchi, Phys. Rev. B **67**, 214420 (2003)
- [8] A. T. Boothroyd, R. Coldea, D. A. Tennant, D. Prabhakaran, L. M. Helme, and C. D. Frost, Phys. Rev. Lett. **92**, 197201 (2004)
- [9] S. P. Bayrakci, I. Mirebeau, P. Bourges, Y. Sidis, M. Enderle, J. Mesot, D. P. Chen, C. T. Lin, and B. Keimer, Phys. Rev. Lett. **94**, 157205 (2005)
- [10] P. Mendels, D. Bono, J. Bobroff, G. Collin, D. Colson, N. Blanchard, H. Alloul, I. Mukhamedshin, F. Bert, A. Amato, and A. D. Hillier, Phys. Rev. Lett. **94**, 136403 (2005)
- [11] J. O. Haerter, M. R. Peterson, and B. S. Shastry, Phys. Rev. Lett. **97**, 226402 (2006)
- [12] C. A. Marianetti and G. Kotliar, Phys. Rev. Lett. **98**, 176405 (2007)
- [13] C. Piefke, L. Boehnke, A. Georges, and F. Lechermann, Phys. Rev. B **82**, 165118 (2010)
- [14] J. Merino, R. H. McKenzie, and B. J. Powell, Phys. Rev. B **80**, 045116 (2009)
- [15] S. Zhou and Z. Wang, Phys. Rev. Lett. **98**, 226402 (2007)
- [16] O. E. Peil, A. Georges, and F. Lechermann, Phys. Rev. Lett. **107**, 236404 (2011)
- [17] H. W. Zandbergen, M. Foo, Q. Xu, V. Kumar, , and R. J. Cava, Phys. Rev. B **70**, 024101 (2004)
- [18] Y. Hinuma, Y. S. Meng, and G. Ceder, Phys. Rev. B **77**, 224111 (2008)
- [19] A. Georges, G. Kotliar, W. Krauth, and M. J. Rozenberg, Rev. Mod. Phys. **68**, 13 (1996)
- [20] T. Maier, M. Jarrell, T. Pruschke, and M. H. Hettler, Rev. Mod. Phys. **77**, 1027 (2005)
- [21] M. D. Johannes, I. I. Mazin, D. J. Singh, and D. A. Papaconstantopoulos, Phys. Rev. Lett. **93**, 097005 (2004)
- [22] M. M. Korshunov, I. Eremin, A. Shorikov, V. I. Anisimov, M. Renner, and W. Brenig, Phys. Rev. B **75**, 094511 (2007)
- [23] K. Kuroki, S. Onari, Y. Tanaka, R. Arita, and T. Nojima, Phys. Rev. B **73**, 184503 (2006)
- [24] H. Alloul, I. R. Mukhamedshin, T. A. Platova, and A. V. Dooglav, Europhys. Lett. **85**, 47006 (2009)
- [25] D. Qian, L. Wray, D. Hsieh, L. Viciu, , R. J. Cava, J. L. Luo, D. Wu, N. L. Wang, and M. Z. Hasan, Phys. Rev. Lett. **97**, 186405 (2006)
- [26] J. Laverock, S. B. Dugdale, J. A. Duffy, J. Wooldridge, G. Balakrishnan, M. R. Lees, G. q. Zheng, D. Chen, C. T. Lin, A. Andrejczuk, M. Itou, and Y. Sakurai, Phys. Rev. B **76**, 052509 (2007)
- [27] H. Rosner, S.-L. Drechsler, G. Fuchs, A. Handstein, A. Wälte, and K.-H. Müller, Braz. J. Phys. **33**, 718 (2003)
- [28] A. N. Rubtsov, V. V. Savkin, and A. I. Lichtenstein, Phys. Rev. B **72**, 035122 (2005)
- [29] P. Werner, A. Comanac, L. de' Medici, M. Troyer, and A. J. Millis, Phys. Rev. Lett. **97**, 076405 (2006)
- [30] M. Ferrero and O. Parcollet, "TRIQS, a Toolkit for Research in Interacting Quantum Systems," To be published
- [31] L. Boehnke, H. Hafermann, M. Ferrero, F. Lechermann, and O. Parcollet, Phys. Rev. B **84**, 075145 (2011)
- [32] V. Zlatić and B. Horvatić, Solid State Comm. **75**, 263 (1990)
- [33] D. Qian, D. Hsieh, L. Wray, Y.-D. Chuang, A. Fedorov, D. Wu, J. L. Lue, N. L. Wang, L. Viciu, R. J. Cava, and M. Z. Hasan, Phys. Rev. Lett. **96**, 216405 (2006)
- [34] Q. Huang, M. L. Foo, J. W. Lynn, H. W. Zandbergen, G. Lawes, Y. Wang, B. H. Toby, A. P. Ramirez, N. P. Ong, and R. J. Cava, J. Phys.: Condens. Matter **16**, 5803 (2004)
- [35] F. L. Ning, S. M. Golin, K. Ahilan, T. Imai, G. J. Shu, and F. C. Chou, Phys. Rev. Lett. **100**, 086405 (2008)
- [36] M. Lee, L. Viciu, L. Li, Y. Wang, M. L. Foo, S. Watauchi, R. A. Pascal, R. J. Cava, and N. P. Ong, Nat. Mat. **5**, 537 (2006)
- [37] G. Gašparović, R. A. Ott, J.-H. Cho, F. C. Chou, Y. Chu, J. W. Lynn, and Y. S. Lee, Phys. Rev. Lett. **96**, 046403 (2006)
- [38] C. Fouassier, G. Matejka, J.-M. Reau, and P. Hagemuller, J. Solid State Chem. **6**, 532 (1973)
- [39] A. V. Kimel, C. D. Stanciu, P. A. Usachev, R. Pisarev, V. N. Gridnev, A. Kirilyuk, and T. Rasing, Phys. Rev. B **74**, 060403(R) (2006)
- [40] H. Alloul, I. R. Mukhamedshin, G. Collin, and N. Blanchard, EPL (Europhysics Letters) **82**, 17002 (2008)
- [41] J. and Koringa, Physica **16**, 601 (1950), ISSN 0031-8914
- [42] T. Moriya, Journal of the Physical Society of Japan **18**, 516 (1963)
- [43] E. Yusuf, B. J. Powell, and R. H. McKenzie, J. Phys.: Condens. Matter **21**, 195601 (2009)
- [44] Note that we use a slightly different definition of χ_s than Ref. [43].
- [45] A further reason could be an additional peak in the corresponding measurement at this precise doping[2], which might or might not be of electronic nature, possibly influencing the Koringa ratio.